Quantitative Analysis of γ′ and η Phase Evolution in a Ni-Based Superalloy Under Laser-Assisted Heat Treatment

Alotaibi Fawaz Marzouq S , Usman Ali * , Atta-Ur Rehman , Talal Ameen Ali Alhemyari

Posted Date: 20 April 2026

doi: 10.20944/preprints202604.1299.v1

Keywords: Ni-based superalloy; γ′ Ni_3(Al,Ti) and η (Ni_3Ti) phase; laser-assisted processing; precipitation behavior; size distribution analysis; microstructure property relationship

 doi:10.20944/preprints202604.1299.v1

Article

Quantitative Analysis of γ′ and η Phase Evolution in a Ni-Based Superalloy Under Laser-Assisted Heat Treatment

Alotaibi Fawaz Marzouq S [1], Usman Ali [2,*], Atta-Ur-Rehman [1] and Talal Ameen Ali Alhemyari [3]

[1] College of Mechanical and Automotive Engineering, South China University of Technology, Guangzhou 510006, China

[2] College of Materials Science and Engineering, Taiyuan University of Technology, Taiyuan 030024, China

[3] Independent Researcher Birmingham, Alabama, USA

* Correspondence: xeensani@gmail.com

Abstract

This study investigates the microstructural evolution and mechanical behavior of a Ni-based superalloy subjected to combined heat treatment and laser processing. Special emphasis is placed on the quantitative analysis of γ′ $Ni_3(Al,Ti)$ and η (Ni_3Ti) phase distributions using SEM-based statistical methods. OM/XRD were employed for initial structural and phase identification, followed by detailed microstructural characterization using SEM/EDS. The results reveal that γ′ precipitates exhibit a fine and uniform distribution with a high number density, whereas the η (Ni_3Ti) phase appears as relatively coarse and sparsely distributed particles. Statistical size distribution analysis demonstrates that processing parameters significantly influence precipitate morphology and phase stability. Laser treatment promotes redistribution of γ′ precipitates and suppresses η (Ni_3Ti) phase formation, resulting in improved microstructural homogeneity. Mechanical characterization shows a strong correlation between γ′ $Ni_3(Al,Ti)$ phase refinement and enhanced hardness and tensile properties. Fractography analysis indicates predominantly ductile fracture behavior with microvoid coalescence. The findings provide a quantitative understanding of phase evolution and establish a microstructure property relationship for optimizing Ni-based superalloys through advanced processing techniques.

Keywords: Ni-based superalloy; γ′ $Ni_3(Al,Ti)$ and η (Ni_3Ti) phase; laser-assisted processing; precipitation behavior; size distribution analysis; microstructure property relationship

1. Introduction

Ni-based superalloys are widely used in high-temperature applications due to their excellent mechanical strength and thermal stability. The superior performance of these alloys is primarily attributed to the presence of γ′ $Ni_3(Al,Ti)$ precipitates, which act as the main strengthening phase. However, the formation of the η (Ni_3Ti) phase during thermal exposure can adversely affect mechanical properties by reducing the availability of strengthening elements. Although numerous studies have investigated precipitation behavior in Ni-based superalloys, most focus on qualitative microstructural observations. Limited work has been conducted on the quantitative statistical analysis of γ′ $Ni_3(Al,Ti)$ and η (Ni_3Ti) phase size distributions, particularly under combined laser and heat-treatment conditions [1–3].

In this study, a comprehensive investigation is conducted to analyze the evolution of the γ′ $Ni_3(Al,Ti)$ and η (Ni_3Ti) phases using SEM-based statistical methods. Furthermore, the influence of laser processing on phase redistribution and mechanical performance is systematically evaluated, providing new insights into microstructural optimization strategies [4,5].

 doi:10.20944/preprints202604.1299.v1

2. Experimental Procedure

The Ni-based superalloy specimens were sectioned and prepared using standard metallographic procedures, including grinding, polishing, and chemical etching using a solution of 20% HF, 10% HNO_3, and 70% H_2O. OM was used for initial microstructural observation, followed by XRD analysis using Co Kα radiation for phase identification. Detailed microstructural characterization was performed using SEM/EDS to examine the morphology and composition of γ' $Ni_3(Al,Ti)$ and η (Ni_3Ti) phases. Quantitative analysis of precipitate size distribution was conducted using image-based statistical methods [6–8].

Laser surface treatment was applied under controlled power and scanning speed conditions to modify the microstructure. Mechanical properties were evaluated through Vickers hardness and tensile testing. Fracture surfaces were analyzed using SEM to identify failure mechanisms [9–12].

3. Result and Discussion

3.1. Initial Microstructure and Phase Identification

The material used in this study is a laboratory-developed Ni-based superalloy, selected due to its excellent high-temperature strength, oxidation resistance, and mechanical stability under extreme service conditions. These properties make it a suitable candidate for aerospace and high-temperature industrial applications. Based on its composition, it can be classified as a Ni-Co-Cr-W-Al-Ti-Nb multicomponent superalloy, strengthened primarily by γ' $Ni_3(Al,Ti)$ precipitates along with solid-solution strengthening from W-Co [13,14].

Table 1. The chemical composition of the Ni-based superalloy (wt.%).

Elements	Co	Cr	W	Al	Ti	Nb	C	Ni
wt.%	20.0	16.5	5.0	2.6	2.5	2.5	0.02	Bal.

Figure 1 shows the optical micrographs and corresponding XRD pattern of the as-processed Ni-Co-Cr-W-Al-Ti-Nb superalloy. The optical images shown in Figure 1a–c reveal a predominantly equiaxed grain structure with well-defined grain boundaries, indicating the formation of a uniform γ matrix during processing. Minor variations in grain size suggest localized heterogeneity. However, no abnormal grain growth is observed, confirming effective microstructural control. The XRD pattern confirms that the γ' $Ni_3(Al,Ti)$ phase is the dominant constituent, with characteristic diffraction peaks corresponding to the (111), (200), (220), and (311) planes of the FCC structure. No significant secondary phases are detected, indicating that the alloy remains in a stable single-phase γ condition in the as-processed state [15–17].

3.2. SEM Microstructure and Phase Distribution

The γ' $Ni_3(Al,Ti)$ phase is the primary strengthening phase in Ni-based superalloys. In the as-processed condition, it exists as fine, coherent precipitates within the γ matrix or as partially coarsened particles depending on prior thermal history. The morphology of γ' evolves from spherical to cuboidal or plate-like with increasing temperature and time. The volume fraction, size, and distribution of γ' precipitates strongly influence mechanical strength, creep resistance, and thermal stability [18]. Figure 2 shows the SEM micrograph and corresponding EDS analysis of the alloy, revealing a continuous γ matrix with a uniform distribution of fine γ' precipitates. The γ' $Ni_3(Al,Ti)$ phase is homogeneously dispersed, indicating effective precipitation during processing. The EDS results confirm a Ni-rich composition with alloying elements such as Cr, Mo, Al, and Ti. Al-Ti contributes to γ' formation, while Cr-Mo provides solid-solution strengthening. The absence of compositional segregation indicates good chemical homogeneity [19,20].

 doi:10.20944/preprints202604.1299.v1

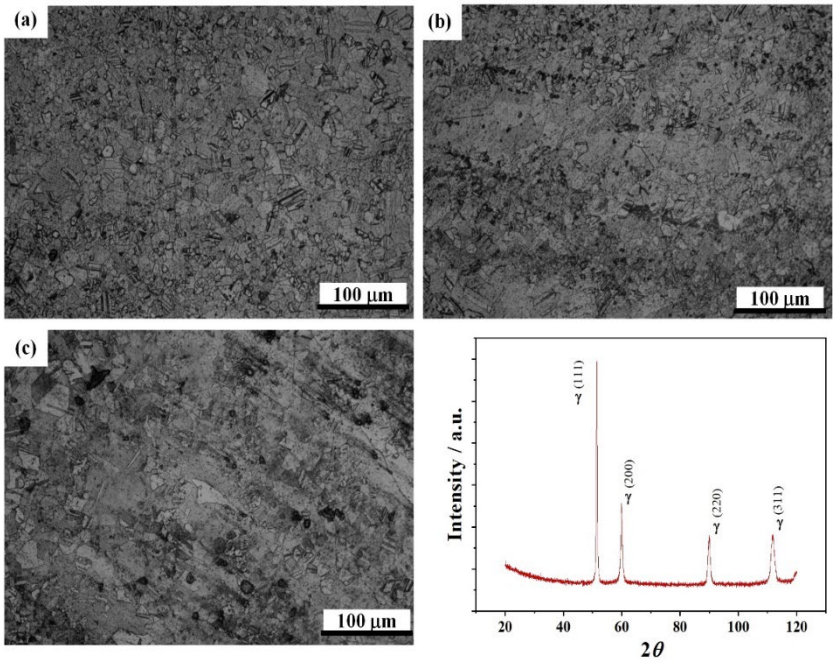

Figure 1. OM microstructure and XRD pattern of the Ni-based superalloy showing the γ matrix with FCC structure.

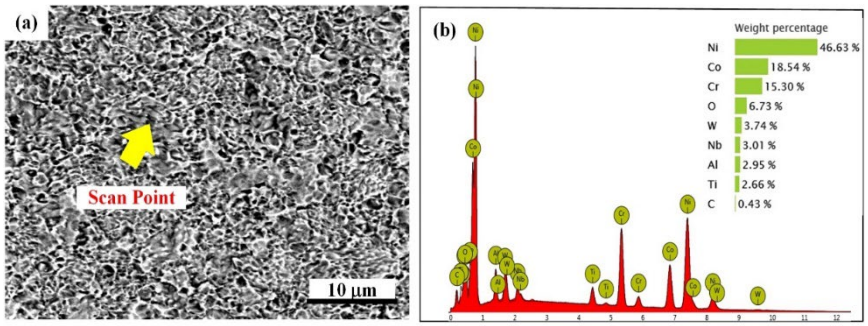

Figure 2. SEM microstructure of the as-processed Ni-based superalloy showing the distribution of γ' precipitates within the γ matrix and the presence of η (Ni_3Ti) phase particles.

3.3. Quantitative Size Distribution Analysis

Figure 3 analyzes the comparative size distribution of η (Ni_3Ti) and γ′ Ni_3(Al,Ti) phase precipitates obtained from SEM-based statistical analysis. The histogram of the η (Ni_3Ti) phase shows that a significant portion of the particles is concentrated within the size range of approximately 0.1-0.4 µm, with the highest counts observed at lower size intervals (222 and 210 particles). However, a noticeable fraction of larger η particles is also present, extending beyond 0.6 µm, indicating a relatively coarser and less uniform distribution. In contrast, the γ′ Ni_3(Al,Ti) phase exhibits a much finer and more densely populated distribution, with a significantly higher number of particles (n = 2916) compared to the η (Ni_3Ti) phase (n = 505). The majority of γ′ precipitates are concentrated in the smaller size range of approximately 0.05-0.3 µm, with peak counts reaching 910 and 925 particles. The frequency decreases progressively with increasing particle size, indicating a typical precipitation-controlled growth behavior [21–23].

 doi:10.20944/preprints202604.1299.v1

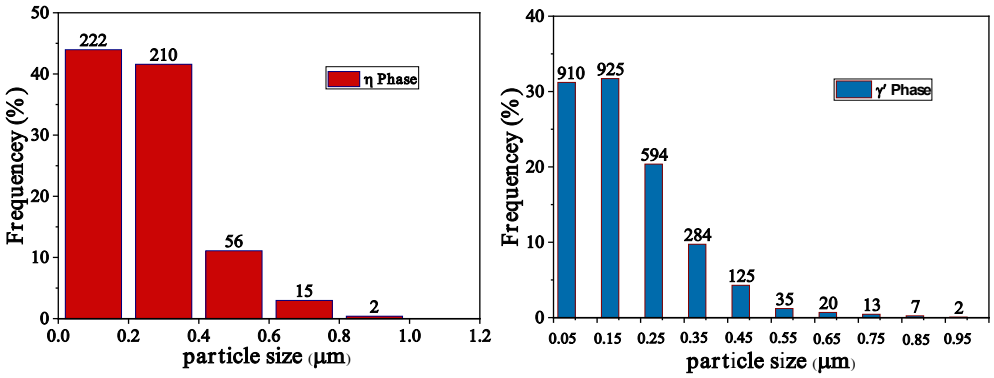

Figure 3. Statistical size distribution of γ' $Ni_3(Al,Ti)$ and η (Ni_3Ti) phase precipitates derived from the SEM microstructure in Figure 2.

The comparison clearly demonstrates that γ′ precipitates are finer and more uniformly distributed, which is beneficial for strengthening as they effectively hinder dislocation motion. On the other hand, the η (Ni_3Ti) phase appears as coarser particles with a lower number density, which may negatively affect mechanical performance by consuming strengthening elements such as Ti-C. Therefore, controlling the formation and growth of the η (Ni_3Ti) phase while promoting fine γ′ precipitation is essential for optimizing the microstructure and mechanical properties of Ni-based superalloys [24].

3.4. Precipitation Behavior During Aging

Heat treatment plays a critical role in optimizing the microstructure, mechanical properties, and high-temperature stability of Ni-based superalloys. It typically involves solution treatment and aging, which control the nucleation, growth, and coarsening of γ′ $Ni_3(Al,Ti)$ precipitates. During solution treatment, existing precipitates and segregated phases dissolve into the γ matrix, resulting in a homogeneous solid solution suitable for subsequent controlled precipitation. Figure 4 illustrates the nucleation behavior after aging at 760 °C for 16 hours. Figure 4a shows a localized precipitate region within the γ matrix, indicating early-stage phase formation. Elemental mapping Figure 4b–e, reveals uniform Ni distribution, with localized enrichment of Ti-Nb within the precipitate, suggesting their key role in phase nucleation and growth [25].

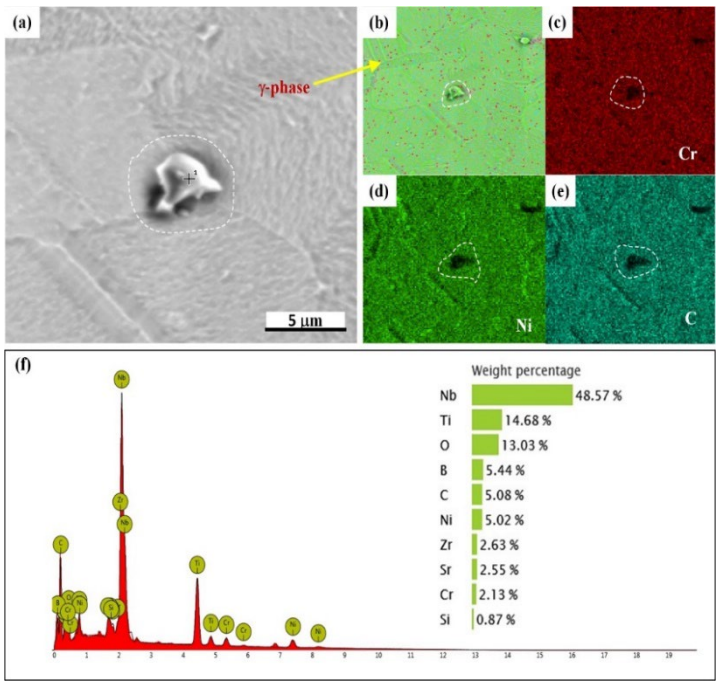

 doi:10.20944/preprints202604.1299.v1

Figure 4. SEM image showing the nucleation and growth behavior of γ' precipitates after aging at 760 °C.

The EDS spectrum Figure 4f confirms high Nb (48.57 wt.%) and Ti (14.68 wt.%) content, indicating that the precipitate is likely a Nb-Ti-rich secondary phase, such as η (Ni_3Ti), rather than a typical γ′ phase. Due to the fine size and coherent nature of γ′ precipitates, they are not clearly distinguishable in SEM at this scale [26–28]. Overall, aging at 760 °C promotes elemental redistribution and localized nucleation, influencing phase evolution and microstructural stability. The homogenized structure obtained after solution treatment ensures effective and controlled precipitation during aging, which is essential for achieving optimal mechanical performance.

3.5. Grain Boundary and Phase Evolution

Figure 5 illustrates the redistribution of γ′ precipitates and suppression of the η (Ni_3Ti) phase after laser-assisted heat treatment. The SEM image shows a remnant η phase particle at the grain boundary, surrounded by a depletion zone, indicating local solute consumption during its formation. Elemental mapping reveals a relatively uniform Ni distribution, while Cr-Co shows slight redistribution near the η (Ni_3Ti) phase. The surrounding γ matrix appears enriched with γ′ precipitates, suggesting that rapid thermal cycling during laser processing promotes partial dissolution of η (Ni_3Ti) phase and solute re-partitioning into the matrix [29].

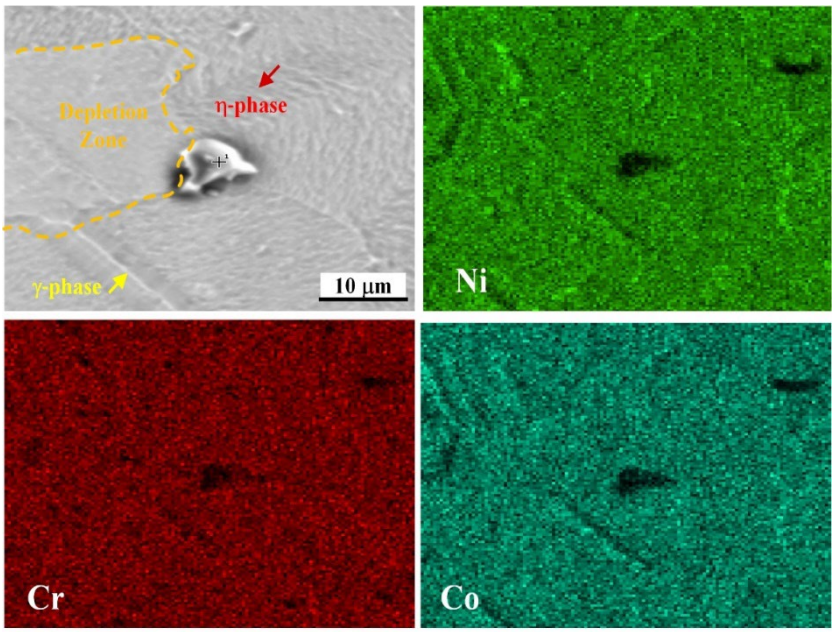

Figure 5. SEM microstructure illustrating grain boundary precipitates and secondary phase formation in the heat-treated alloy.

This redistribution enhances γ′ stabilization while inhibiting further η (Ni_3Ti) phase growth. Overall, the results demonstrate that laser treatment effectively modifies local chemical gradients, suppresses detrimental η (Ni_3Ti) phase formation, and promotes γ′ precipitation, leading to improved microstructural stability [30].

Upon aging, fine γ′ precipitates re-form uniformly within the matrix. Aging promotes controlled γ′ $Ni_3(Al,Ti)$ phase nucleation and growth within the supersaturated γ matrix. The size, distribution, and volume fraction of γ′ $Ni_3(Al,Ti)$ phase after aging determine yield strength and creep resistance. Multi-stage aging produces bimodal distributions that combine fine and coarse precipitates for optimal mechanical performance. Figure 6 shows SEM micrographs and corresponding EDS analyses illustrating the evolution of grain boundary precipitates under different heat-treatment conditions [31–33].

 doi:10.20944/preprints202604.1299.v1

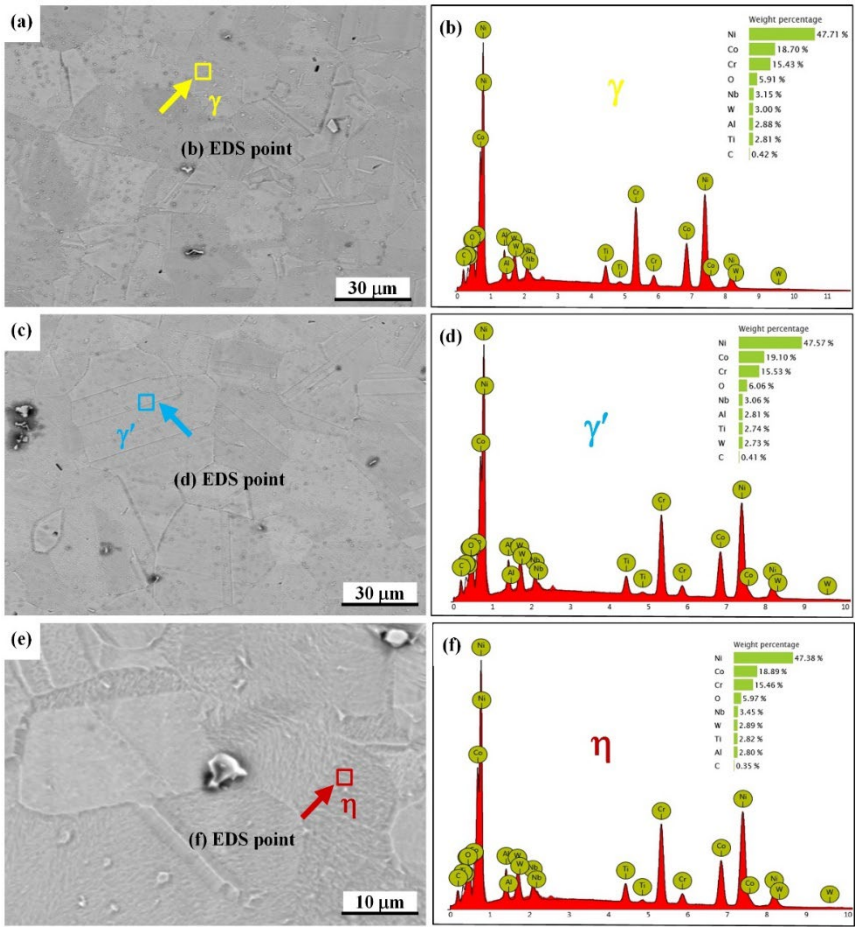

Figure 6. Microstructural evolution showing suppression of η (Ni_3Ti) phase and redistribution of γ' precipitates under heat treatment conditions.

In the solution-treated condition, the microstructure is dominated by the γ matrix, as shown in Figure 6a,b with EDS analysis at point, confirming a Ni-rich composition characteristic of the γ phase. After aging, discrete γ′ precipitates are observed near grain boundaries, as shown in (c, d), and the corresponding EDS spectrum reveals enrichment of γ′ forming elements such as Al, Ti, and Nb, confirming the formation of the γ′ Ni_3(Al,Ti) phase. With further heat treatment, coarser grain boundary precipitates identified as the η (Ni_3Ti) phase appear, as shown in (e, f). The EDS result indicates increased Nb-Ti contents together with reduced Ni, consistent with η (Ni_3Ti) phase formation. These results demonstrate that heat treatment strongly influences the type, composition, and morphology of grain boundary precipitates, with a progression from γ to γ′ Ni_3(Al,Ti) and eventually to η (Ni_3Ti) phase, which plays a critical role in controlling grain boundary stability and mechanical properties of the alloy [34].

3.6. Effect of Laser Processing

Laser processing induces multiple microstructural modifications in Ni-based alloys. Figure 7 shows SEM micrographs with corresponding EDS point analyses illustrating the elemental distribution after laser-assisted heat treatment. In Figure 7a, η (Ni_3Ti) phase precipitates are observed along grain boundaries, as indicated by the red arrows, while the surrounding matrix is identified as the γ′ Ni_3(Al,Ti) phase. The EDS spectrum taken from the η (Ni_3Ti) phase region, Figure 7c, shows enrichment of Ti-Al with reduced Ni content, which is characteristic of the η (Ni_3Ti) phase [35].

 doi:10.20944/preprints202604.1299.v1

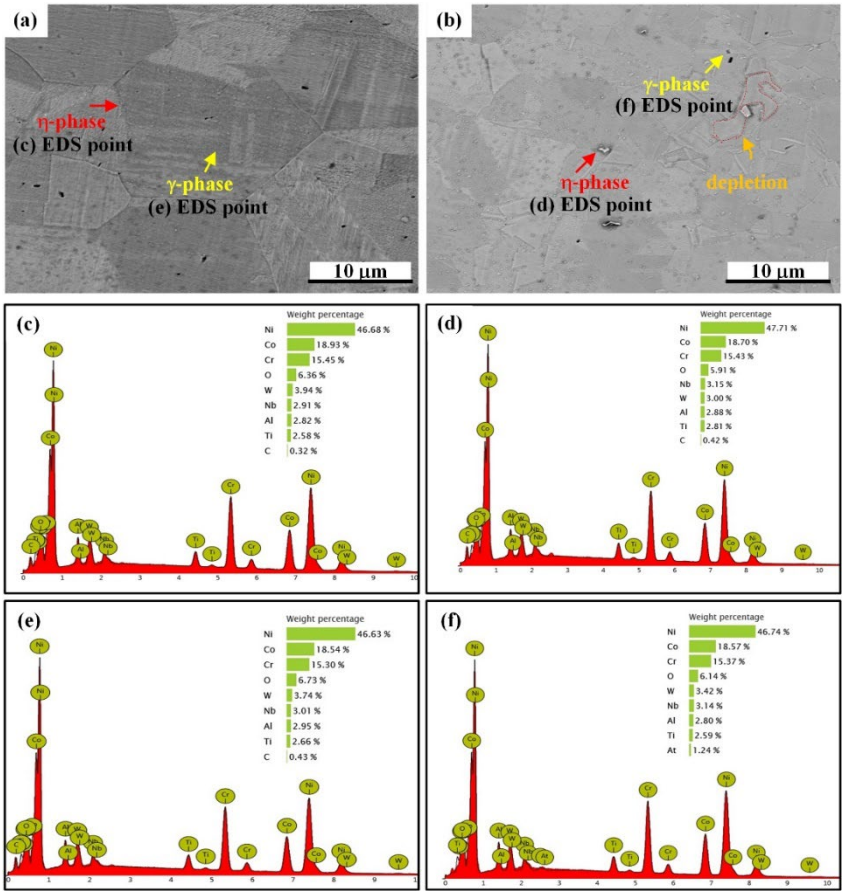

Figure 7. SEM/EDS analysis of the laser-treated alloy showing elemental distribution and phase identification.

In contrast, the EDS analysis of the adjacent γ′ Ni_3(Al,Ti) phase region in Figure 7e confirms a Ni-rich composition with comparatively lower concentrations of Ti-Al. In (b), a similar microstructural configuration is observed. However, a distinct elemental depletion zone is evident near the η precipitate, as marked by the dashed region. The EDS spectrum from the η (Ni_3Ti) phase in Figure 7d again demonstrates Ti-Al enrichment, whereas the γ phase spectrum in Figure 7f indicates local depletion of these γ′ Ni_3(Al,Ti) phase-forming elements. These results suggest that laser treatment promotes elemental redistribution through rapid thermal cycling, leading to solute partitioning toward η precipitates and the formation of depletion zones in the surrounding γ matrix, which may significantly influence local phase stability and mechanical behavior [36–38].

Figure 8 presents the size distribution of γ′ Ni_3(Al,Ti) precipitates for Sample-1 and Sample-2 obtained from SEM analysis. The γ′ precipitates are predominantly distributed within the submicron range (0.1-0.4 μm), with a high frequency of fine particles, indicating effective precipitation during aging. Sample-2 exhibits a slightly higher fraction of finer precipitates (~0.1-0.2 μm), suggesting a more refined microstructure, whereas Sample-1 shows a comparatively broader distribution with a higher proportion of larger particles. The distribution follows a right-skewed trend, with frequency decreasing as particle size increases, characteristic of diffusion-controlled precipitate growth. The presence of fine and uniformly distributed γ′ precipitates enhances strengthening by effectively impeding dislocation motion [39,40].

In contrast, the η (Ni_3Ti) phase exhibits a coarser size distribution, primarily within the range of 0.5-1.2 μm, with peak frequency around 0.8-1.0 μm. Compared to γ′, the larger size of η precipitates reflects their preferential growth during aging. Sample-2 shows a slightly higher frequency within this dominant size range, indicating an increased tendency for η phase formation or coarsening under the given processing conditions. Overall, the results demonstrate that processing parameters

 doi:10.20944/preprints202604.1299.v1

significantly influence precipitate size distribution, where finer γ′ promotes strengthening, while coarser η (Ni_3Ti) phase may adversely affect mechanical performance [40–43].

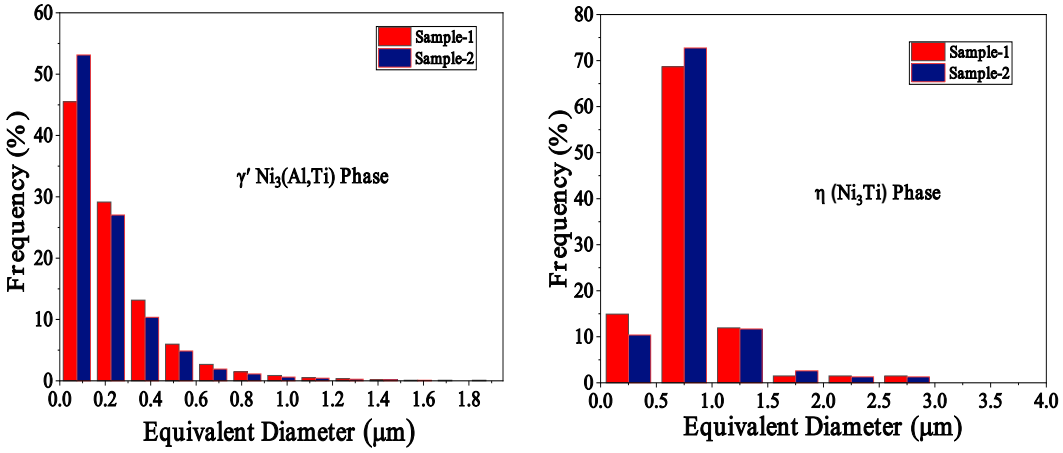

Figure 8. Comparative statistical size distribution of γ' and η (Ni_3Ti) phase precipitates derived from the SEM microstructure of the laser.

Laser processing creates depth-dependent gradients in microstructure. Figure 9 compares SEM micrographs illustrating the effect of varying laser power and scanning speed on the morphology and distribution of γ′ precipitates [44,45]. At lower laser power (155 W), the microstructure shows relatively fine and uniformly distributed γ′ precipitates at scanning speeds of 0.7 and 1.0 m/s, whereas increasing the scanning speed to 1.3 m/s results in the appearance of localized agglomeration and microstructural heterogeneity, as highlighted by the dashed regions. At an intermediate laser power of 170 W, a more homogeneous γ′ Ni_3(Al,Ti) phase distribution is observed across all scanning speeds, with minimal evidence of coarsening or clustering, indicating optimized thermal input and cooling rates for γ′ Ni_3(Al,Ti) phase stabilization [46–50]. At the highest laser power (195 W), the γ′ precipitates remain uniformly dispersed at lower scanning speeds. However, slight coarsening and redistribution become noticeable at higher speeds due to enhanced thermal gradients and rapid solidification effects. The relative density values annotated in each condition remain high, suggesting that the observed microstructural differences are primarily governed by thermal-kinetic effects rather than porosity. The results demonstrate that laser power plays a critical role in controlling γ′ precipitate morphology, with intermediate power conditions providing the most uniform and stable γ′ Ni_3(Al,Ti) phase microstructure [51–55].

The relative density increases with scanning speed for all laser power levels. Figure 10 shows that with a lower scanning speed (0.7 m/s), the density is comparatively low, particularly at 170 W. As the scanning speed increases to 1.0 m/s, a significant improvement in densification is observed, with the highest relative density achieved at 170 W. At 1.3 m/s, the density values for 170 W and 195 W converge, indicating near-optimal processing conditions. Overall, an optimal combination of laser power and scanning speed enhances densification, while lower speeds result in insufficient energy distribution and reduced density [56–61].

3.7. Mechanical Properties

Table 2 shows the nominal chemical composition of the investigated Ni-based superalloy samples in wt.%. All samples exhibit a Ni-rich composition with significant additions of Co-Cr, which contribute to solid solution strengthening and corrosion resistance. The presence of Al-Ti promotes the formation of γ′ Ni_3(Al,Ti) strengthening precipitates, while Nb supports the formation of secondary phases. Minor variations in elemental content among the samples, particularly in C, Nb, and O, are expected to influence phase evolution, precipitation behavior, and mechanical properties.

 doi:10.20944/preprints202604.1299.v1

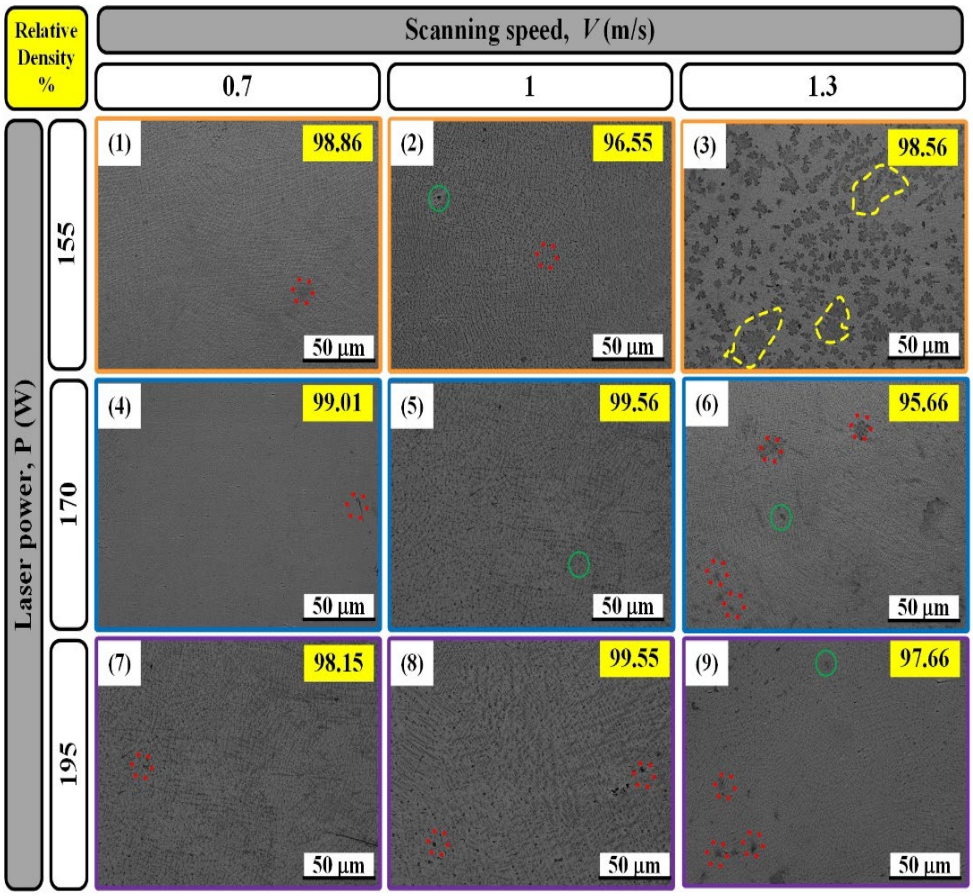

Figure 9. SEM microstructure showing improved densification and microstructural homogeneity after laser processing.

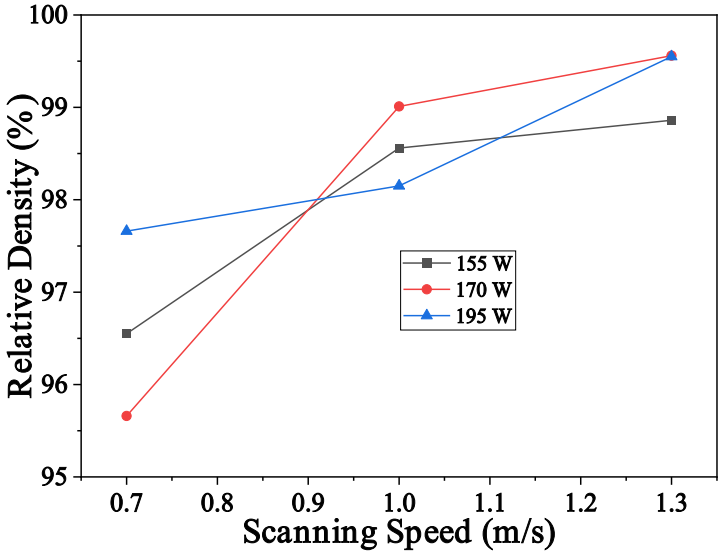

Figure 10. Effect of laser processing parameters (170 W, 1.0 m/s) on microstructural refinement and phase stability.

Table 2. Nominal chemical composition of our samples of the Ni-based superalloys, with wt.% as the major variant.

Samples	Ni	Co	Cr	O	W	Nb	Al	Ti	C
1	46.63	18.54	15.30	6.73	3.74	3.01	2.95	2.66	0.43
2	46.74	18.57	15.37	6.14	3.42	3.12	2.80	2.59	1.24

 doi:10.20944/preprints202604.1299.v1

3	46.68	18.93	15.45	6.36	3.94	2.91	2.82	2.58	0.32
4	47.71	18.70	15.43	5.91	3.15	3.00	2.88	2.81	0.42

A limited and well-dispersed η (Ni_3Ti) phase can enhance creep resistance by impeding dislocation motion and stabilizing γ′ precipitates; however, excessive growth or continuous η formation along grain boundaries promotes brittleness and accelerates creep failure. Figure 11 shows the variation of Vickers hardness (HV) with temperature for different aging times (1, 2, 4, and 8 hours), highlighting a strong dependence on thermal exposure and aging duration. The 2-hours condition exhibits the highest hardness (~525 HV at 300 °C), indicating optimal precipitation strengthening due to fine and uniformly distributed γ′ precipitates. With increasing temperature, hardness decreases to ~510 HV at 500 °C, followed by a slight increase (~515 HV at 600 °C), likely due to secondary precipitation or precipitate redistribution. A significant drop (~485 HV) at 700 °C indicates precipitate coarsening and reduced strengthening efficiency. The 1-hour condition shows lower initial hardness (~455 HV at 300 °C) but increases to ~495 HV at 600 °C, suggesting incomplete precipitation at shorter aging times. In contrast, the 4 and 8 hours conditions exhibit progressive hardness reduction with temperature (≈480→455 HV and ≈495→475 HV, respectively), reflecting over-aging and γ′ coarsening. Prolonged exposure also promotes η (Ni_3Ti) phase formation, further degrading hardness. Overall, the 2-hours aging condition provides optimal strengthening, whereas higher temperatures and extended aging lead to microstructural coarsening and reduced hardness [62].

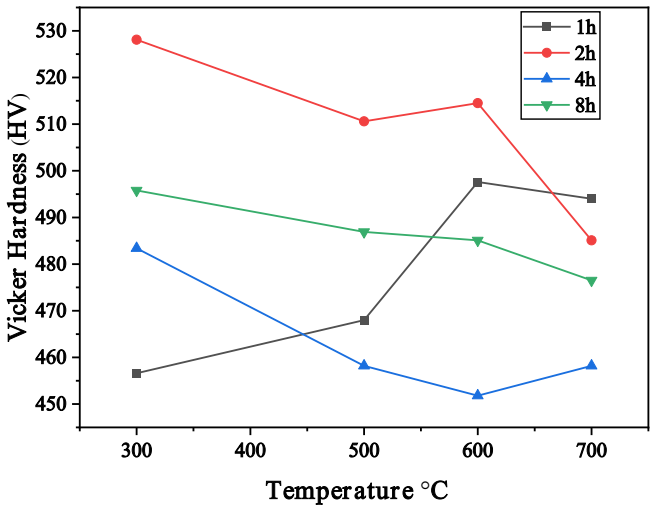

Figure 11. Variation in microhardness of the Ni-based superalloy as a function of microstructural evolution and γ′ $Ni_3(Al,Ti)$ phase refinement.

Fully optimized aging heat treatments generate the highest yield strength due to high anti-shearing resistance by dislocation cutting mechanisms. Inadequate heat treatment yields insufficient precipitation, whereas over-aging causes γ′ $Ni_3(Al,Ti)$ phase growth and weakening of precipitation strengthening. High-temperature tensile strength is controlled by the stability of the γ′ $Ni_3(Al,Ti)$ phase at elevated temperatures. Proper heat treatment improves creep strength, dislocation drag force, and delays rafting formation [63,64]. At higher temperatures, the deformation mechanism shifts from isothermal to dislocation climb or bypassing. This improvement is mainly attributed to the precipitation of strengthening phases, which effectively impede dislocation motion during deformation. Figure 12(b) compares the YS and UTS of the aged samples, showing YS values in the range of about 1000-1150 MPa and corresponding UTS values between 1300-1500 MPa. Among the samples, sample 3 exhibits the highest tensile strength, suggesting a more favorable microstructural condition resulting from aging [65–67].

 doi:10.20944/preprints202604.1299.v1

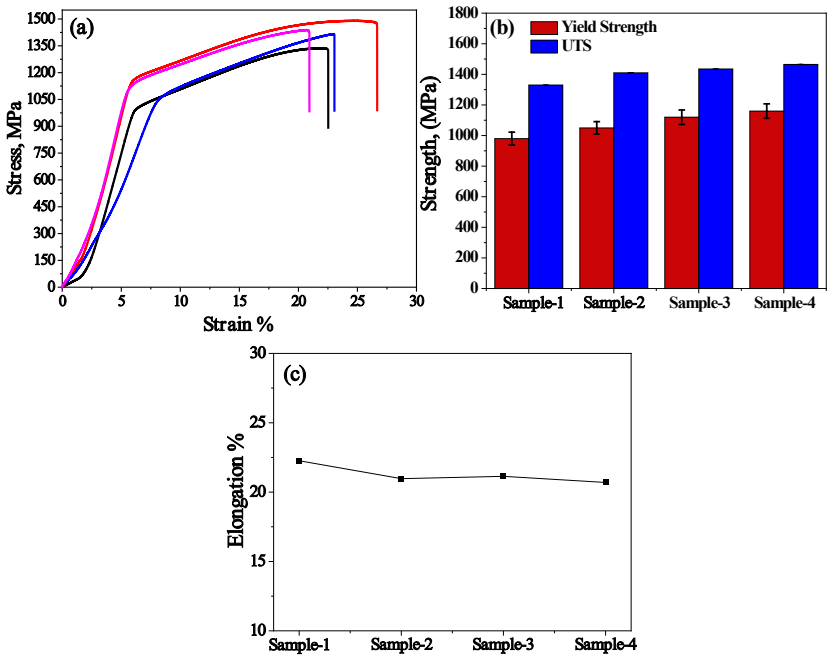

Figure 12. Tensile properties of the alloy showing the relationship between microstructure and mechanical performance.

The elongation to fracture, presented in Figure 12c, ranges from approximately 20 to 24%, indicating that the alloy retains good ductility despite its high strength. A slight reduction in elongation is observed with increasing strength, reflecting the typical strength-ductility trade-off. Overall, the results confirm that aging treatment significantly enhances the tensile strength of the Ni-based superalloy while maintaining acceptable ductility, making it suitable for high-temperature structural applications [68,69].

3.8. Fracture Behavior

Heat treatment plays a crucial role in tailoring the microstructure and enhancing the mechanical and thermal properties of Ni-based superalloys. The primary objectives include homogenization of composition, dissolution of undesirable phases, and controlled precipitation of strengthening phases such as γ′ and γ″. Different heat treatment processes, including solution treatment, annealing, sub-solution treatment, and aging, are employed to achieve an optimal balance between strength and ductility [70]. Figure 13 shows fractographic SEM images of the Ni-based superalloy, illustrating the fracture characteristics associated with the γ matrix and γ′ precipitates. The low-magnification images reveal a rough and heterogeneous fracture surface, indicating multiple crack initiation sites.

High-magnification images show well-defined cracks within the γ matrix, accompanied by microvoids and tear ridges. These features suggest that crack initiation primarily occurs in the γ′ Ni_3(Al,Ti) phase, while γ′ precipitates act as obstacles to crack propagation. The presence of microvoid coalescence and localized tearing indicates a mixed fracture mode, combining ductile deformation with localized brittle behavior [71].

Figure 14 shows SEM micrographs of the aged Ni-based superalloy, revealing the deformation microstructure at room temperature. The fracture surfaces in all conditions exhibit a predominantly ductile morphology characterized by a dense network of slip traces and dimples, indicating extensive plastic deformation before failure. In Figure 14a,b, the γ matrix is clearly observed, within which localized deformation bands and elongated features are present, suggesting active dislocation motion and strain localization during tensile loading [72].

 doi:10.20944/preprints202604.1299.v1

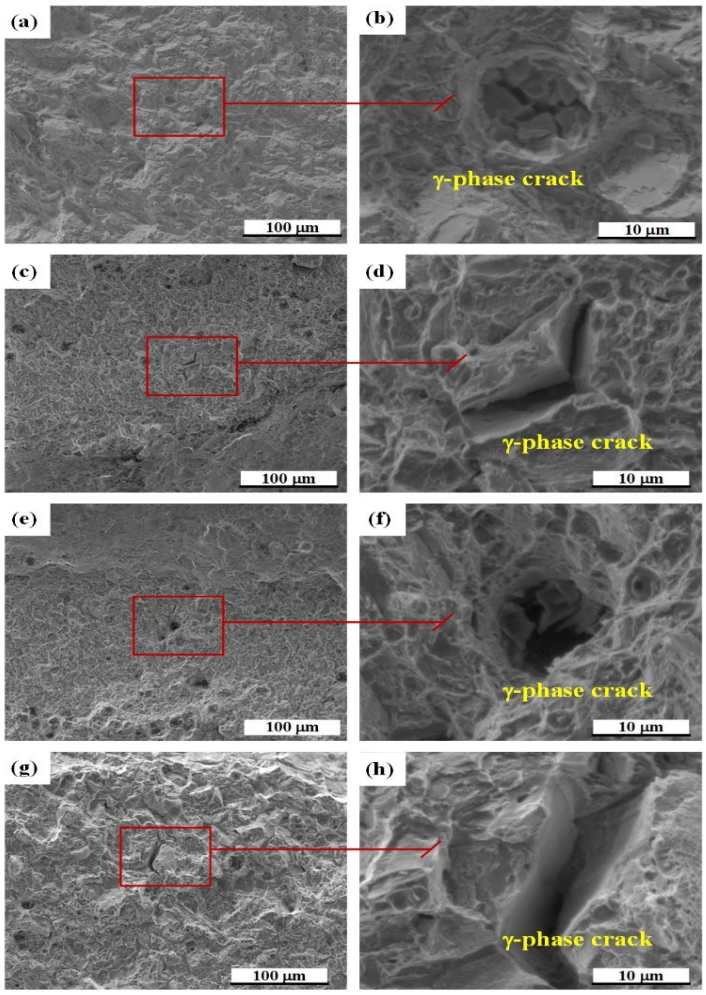

Figure 13. SEM fractography of the tensile-tested specimen showing the overall fracture morphology.

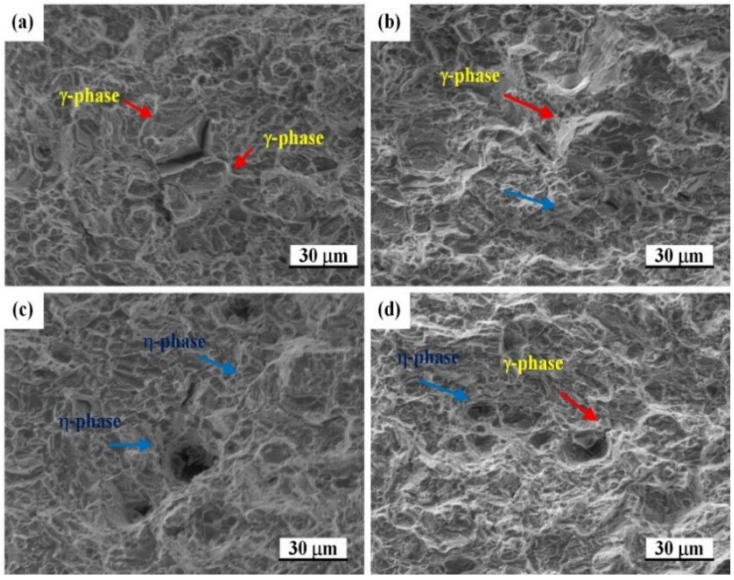

Figure 14. SEM image showing ductile fracture characteristics with prominent plastic deformation features.

Figure 14c highlights the presence of η (Ni_3Ti) phase particles embedded in the γ matrix. These particles act as strong obstacles to dislocation movement, leading to dislocation pile-up and localized stress concentration. In Figure 14d, both the γ′ $Ni_3(Al,Ti)$ and η (Ni_3Ti) phases are observed simultaneously, demonstrating the alloy's heterogeneous microstructure after aging. The interaction

 doi:10.20944/preprints202604.1299.v1

between moving dislocations and the precipitated η (Ni_3Ti) phase contributes significantly to the strengthening mechanism, while the surrounding γ matrix accommodates plastic deformation. Overall, the observed dislocation FCC structures and phase interactions confirm that precipitation strengthening and dislocation hindrance dominate the room-temperature tensile behavior of the aged Ni-based superalloy [73–75].

Figure 15 shows the fracture surface of the alloy after aging at 760 °C for 16 hours. The surface exhibits characteristic features of ductile fracture, including dimples and microvoid coalescence, indicating significant plastic deformation before failure. The presence of fine and uniformly distributed dimples suggests effective precipitation strengthening due to γ′ Ni_3(Al,Ti) phase formation. In some regions, relatively larger dimples and localized features may be observed, which can be attributed to the presence of coarse precipitates or inclusions acting as nucleation sites for void formation. Overall, the fracture morphology confirms that the alloy retains good ductility and toughness after the applied heat treatment.

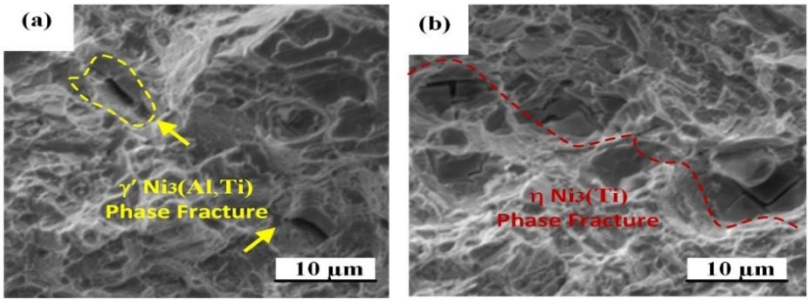

Figure 15. High-magnification SEM image showing dimples and microvoid coalescence on the fracture surface.

Figure 16 shows a schematic illustration of the behavior of γ particles in a Ni-based alloy during solidification. In the melt (top-left), γ particles diffuse randomly, as indicated by the yellow paths. At the solidification front (top-right), particles experience forces: the solidification push FPF-PFP, radial forces from the surrounding melt, and the resultant force FFF, which governs whether particles are engulfed or pushed. In the alloy (bottom-left), the moving solidification front interacts with γ particles, generating local stress and strain fields (curved lines) that influence particle distribution. Finally, at the interface (bottom-right), γ particles accumulate, forming a reinforced microstructure that can enhance the alloy's mechanical properties.

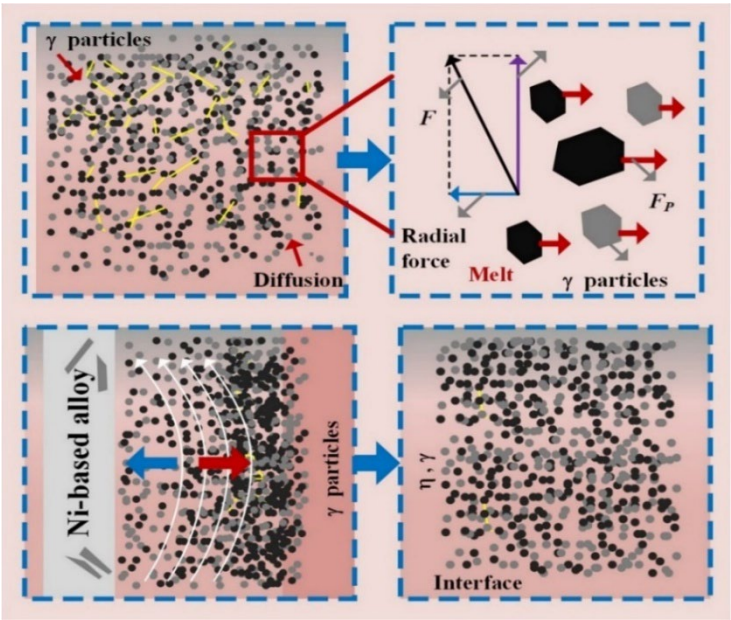

 doi:10.20944/preprints202604.1299.v1

Figure 16. SEM image showing intergranular fracture features and crack propagation along grain boundaries.

4. Key Scientific Finding

The refinement of γ′ precipitates and suppression of η (Ni_3Ti) phase through optimized laser and heat treatment conditions significantly enhance the mechanical performance of the alloy by improving resistance to dislocation motion and delaying crack initiation.

5. Conclusion

In this study, the evolution of γ′ $Ni_3(Al,Ti)$ and η (Ni_3Ti) phases in a Ni-based superalloy under combined heat treatment and laser processing was systematically investigated. The results demonstrate that γ′ precipitates exhibit a fine and uniform distribution, whereas the η (Ni_3Ti) phase forms as coarse particles with a lower number density. Quantitative statistical analysis revealed that processing parameters strongly influence phase morphology and distribution. Laser treatment effectively promotes γ′ redistribution and suppresses η (Ni_3Ti) phase formation, leading to improved microstructural homogeneity. Mechanical testing confirms that the refinement of γ′ precipitates significantly enhances hardness and tensile strength. Fractography analysis indicates predominantly ductile fracture behavior. Overall, this study provides a quantitative framework for tailoring microstructure and improving the performance of Ni-based superalloys.

References

1. RAO Y. FIRST PRINCIPLES THERMODYNAMICS OF METALLIC ALLOYS [M]. THE OHIO STATE UNIVERSITY, 2020.
2. ZHAO Y, HE S, LI L. APPLICATION OF HOT ISOSTATIC PRESSING IN NICKEL-BASED SINGLE CRYSTAL SUPERALLOYS [J]. CRYSTALS, 2022, 12(6): 805.
3. LU H, YANG M, ZHOU L, et al. Effects of Heat Treatment on the Microstructure and Properties of a Cast Nickel-Based High-Cr Superalloy [J]. Metals, 2022, 12(12).
4. LIU J, YANG H-Y, ZHONG X-M, et al. Microstructure manipulation and high-temperature service performance enhancement of nickel-based superalloys [J]. Journal of Materials Research and Technology, 2025.
5. SELVARAJ S K, SUNDARAMALI G, JITHIN DEV S, et al. Recent advancements in the field of Ni-based superalloys [J]. Advances in Materials Science and Engineering, 2021, 2021(1): 9723450.
6. QIAO S, LIU S, LI N, et al. Abnormal grain growth in the Ni-based wrought superalloy GH4698 bar during heat treatment [J]. Journal of Materials Research and Technology, 2024, 30: 6563-75.
7. JAJI N-D, LEE H L, HUSSIN M H, et al. Advanced nickel nanoparticles technology: From synthesis to applications [J]. Nanotechnology reviews, 2020, 9(1): 1456-80.
8. DAI Z, ZHOU J, WANG X, et al. High-quality surface preparation of inconel 718 nickel-based superalloy considering chemical mechanical polishing [J]. International Journal of Precision Engineering and Manufacturing-Green Technology, 2026, 13(1): 49-64.
9. ADAPA V S K, KALIDINDI S R, SALDANA C J. Insights into the gamma prime precipitation behavior during heat treatment of additively manufactured nickel-based superalloy [J]. Journal of Alloys and Compounds, 2025, 1012: 178507.
10. HASHEMI S M, PARVIZI S, BAGHBANIJAVID H, et al. Computational modelling of process–structure–property–performance relationships in metal additive manufacturing: a review [J]. International Materials Reviews, 2022, 67(1): 1-46.
11. SHAO G, XUAN W, ZHAO D, et al. Oxide formation and growth mechanisms for protecting nickel-based IN718 superalloys at elevated temperatures [J]. Materials Characterization, 2025: 115828.
12. SOARES C G, SANTOS T A. Advances in maritime technology and engineering [M]. CRC Press, Taylor & Francis Group, 2024.
13. PRASHAR G T K, SINGH S, SINGH P, SRIVASTAVA VK. Superalloys for high-temperature applications: An overview. [J]. InAIP Conference Proceedings, 2024, Vol. 2986, No. 1, p. 020022.

 doi:10.20944/preprints202604.1299.v1

14. GAO Y, CUI J, DONG J, et al. Revealing the effect of Ta on coarsening behavior of γ′ phases during thermal exposure at 1000 ℃ in a Ni-based SX superalloy [J]. Journal of Alloys and Compounds, 2025, 1010.
15. WANG H, LONG H, LIU Y, et al. The widening of the solution heat treatment window by the addition of Ru in Ni-based single crystal superalloy [J]. Materials Characterization, 2023, 203.
16. FAN Z, GAO F. Grain Initiation and Grain Refinement: An Overview [J]. Metals, 2022, 12(10).
17. NASIRI Z, GHAEMIFAR S, NAGHIZADEH M, et al. Thermal Mechanisms of Grain Refinement in Steels: A Review [J]. Metals and Materials International, 2020, 27(7): 2078-94.
18. FAN Z, GAO F, WANG Y, et al. Effect of solutes on grain refinement [J]. Progress in Materials Science, 2022, 123(123:100809.).
19. GE H, LIU G, ZHENG S, et al. Dislocation climbing dominated decomposition and fracture of carbides in a Ni-based superalloy [J]. Acta Materialia, 2023, 246(246:118669.).
20. ZHANG L, YANG Q, CHEN J, et al. Precipitation and strengthening behavior of η phase in polycrystalline Ni-based superalloy [J]. Materials Science and Engineering: A, 2025, 933(148302).
21. IQBAL M A, SKOTNICOVÁ K, SHAFIQ A, et al. Inconel alloys: A comprehensive review of properties and advanced manufacturing techniques [J]. International Journal of Thermofluids, 2025, 29(101394.).
22. XU Y, TAN Z, WANG X, et al. Increased long-term stress-rupture life of a nickel-based superalloy with relatively homogeneous duplex grain size distributions [J]. Materials & Design, 2024, 244: 113129.
23. ELAIYARASAN U, SATHEESHKUMAR V, SENTHILKUMAR C. Effect of sintered electrode on microhardness and microstructure in electro discharge deposition of magnesium alloy [J]. Journal of the Mechanical Behavior of Materials, 2020, 29(1): 69-76.
24. MUSTAFA G, LI B, ZHANG S. Cutting condition effects on microstructure and mechanical characteristics of Ni-based superalloys—a review [J]. The International Journal of Advanced Manufacturing Technology, 2024, 130(7): 3179-209.
25. MUKHERJEE S, SIVAPRASAD S, TARAFDER S, et al. Influence of ageing on high temperature tensile deformation of a Ni-based superalloy, HAYNES 282 [J]. Journal of Alloys and Compounds, 2022, 917(165430).
26. WU Y, LI C, XIA X, et al. Precipitate coarsening and its effects on the hot deformation behavior of the recently developed γ′-strengthened superalloys [J]. Journal of Materials Science & Technology, 2021, 67: 95-104.
27. YAMAGUCHI Y, TAJIMA R, TERADA Y. Morphology Evolution of γ′ Precipitates for Wrought Ni-Based Superalloys [J]. Materials Transactions, 2020, 61(11): 2185-94.
28. ALI U, QURASHI M S, LARTEY P O, et al. Carbon and Titanium Effect on Tensile Behavior of Aged A286 Nickel-Iron Based Superalloy [J]. Key Engineering Materials, 2023, 963: 3-9.
29. ZHANG X, SHANG H, GAO Q, et al. Coarsening Evolution of γ′ Phase and Failure Mechanism of Co-Ni-Al-Ti-Based Superalloys During Isothermal Aging [J]. Frontiers in Materials, 2022, 9.
30. HUANG Y S, WANG X G, CUI C Y, et al. The effect of coarsening of γ′ precipitate on creep properties of Ni-based single crystal superalloys during long-term aging [J]. Materials Science and Engineering: A, 2020, 773.
31. SHAJARI Y, RAZAVI S H, SEYEDRAOUFI Z S, et al. The Effect of Time and Temperature of Solutionizing Heat Treatment on γ′ Characterization in a Ni-Base Superalloy [J]. Metallography, Microstructure, and Analysis, 2021, 10(4): 441-7.
32. ATAS M S, CENGIZ R, YILDIRIM M. Microstructural Evolution and Coarsening in Ni–Al–Cr–Co Model Superalloys with Nano γ′-Precipitates: An Experimental and Thermodynamic Investigation [J]. Metallography, Microstructure, and Analysis, 2024, 13(4): 582-94.
33. LI P, CHEN L, BU H, et al. Effect of cooling rate on the Morphological changes in the secondary γ′ precipitation in FGH97 nickel-based PM superalloy [J]. Intermetallics, 2024, 171.
34. HE C, LIU L, HUANG T, et al. Effect of aging temperature on the secondary γ′ precipitation in a model Ni based single crystal superalloy [J]. Journal of Alloys and Compounds, 2020, 836.
35. ZHANG J, LIU L, HUANG T, et al. Coarsening kinetics of γ′ precipitates in a Re-containing Ni-based single crystal superalloy during long-term aging [J]. Journal of Materials Science & Technology, 2021, 62: 1-10.

 doi:10.20944/preprints202604.1299.v1

36. GONG X, LIU G, GAO Z, et al. Influence of initial microstructure on the γ′-coarsening behavior in a corrosion-resistant Ni-based superalloy [J]. Intermetallics, 2024, 172.
37. LI H, CHEN W, FANG N, et al. Precipitation of η phase in a nickel based superalloy during aging [J]. Journal of Materials Research and Technology, 2025, 39: 1953-9.
38. CHU D-J, PARK C, LEE J, et al. Formation of eta phase during aging at 750–850 °C for Ni-base superalloys with different Ti/Al ratios [J]. Calphad, 2024, 87.
39. JIN J, ZHAO X, ZHAO Q, et al. Morphology control of η phase in enhancing high-temperature tensile property of superalloy GH4350 [J]. Journal of Alloys and Compounds, 2025, 1024.
40. DONG C, LIU Z, CHEN Z, et al. Carbide dissolution and grain growth behavior of a nickel-based alloy without γ′ phase during solid solution [J]. Journal of Alloys and Compounds, 2020, 825.
41. HOU K, WANG M, ZHAO P, et al. Temperature-dependent yield strength and deformation mechanism of a casting Ni-based superalloy containing low volume-fraction γ′ phase [J]. Journal of Alloys and Compounds, 2022, 905.
42. ALI U, QURASHI M S, LARTEY P O, et al. Influence of η-(Ni3Ti) and TiC phases on corrosion resistance and mechanical properties of A286 austenitic superalloy after heat treatment [J]. International Journal of Electrochemical Science, 2023, 18(7).
43. HU H, ZHAO M, RONG L. Retarding the precipitation of η phase in Fe-Ni based alloy through grain boundary engineering [J]. Journal of Materials Science & Technology, 2020, 47: 152-61.
44. SUN X, CHEN M, LIU T, et al. Characterization, preparation, and reuse of metallic powders for laser powder bed fusion: a review [J]. International Journal of Extreme Manufacturing, 2023, 6(1).
45. FENG Y, LIU B, WAN X, et al. Influence of processing parameter on phase transformation and superelastic recovery strain of laser solid forming NiTi alloy [J]. Journal of Alloys and Compounds, 2022, 908.
46. LIU G, XIAO X, VÉRON M, et al. The nucleation and growth of η phase in nickel-based superalloy during long-term thermal exposure [J]. Acta Materialia, 2020, 185: 493-506.
47. ZHU L, WEI B, XIAO L, et al. Temperature dependence of tensile deformation behaviors in a novel powder metallurgy Ni-based superalloy with high density nanoscale γ′ phase [J]. Materials Science and Engineering: A, 2025, 943.
48. SONG F, LIN X. Laser Cleaning [M]. Springer Singapore, 2024.
49. LI C, HAN X, ZHANG D, et al. Quantitative analysis and experimental study of the influence of process parameters on the evolution of laser cladding [J]. Journal of Adhesion Science and Technology, 2021, 36(17): 1894-920.
50. WANG Q. Laser Additive Manufacturing in Oil and Gas Field Applications [M]. 2025.
51. ZHANG G, HUA X, HUANG Y, et al. Investigation on mechanism of oxide removal and plasma behavior during laser cleaning on aluminum alloy [J]. Applied Surface Science, 2020, 506.
52. YI C, CHEN X, ZHOU Y, et al. Effects of scanning speed and scanning times on surface quality of line spot laser polishing of nickel-based superalloys [J]. Journal of Materials Research and Technology, 2023, 26: 2179-90.
53. WANG W, WANG X, LIU W, et al. Study on surface quality of laser cleaning of oxide film on nickel-base superalloy [J]. Applied Physics A, 2022, 128(3).
54. JIAN Y, LIU Y, QI H, et al. Effects of scanning speed on the microstructure, hardness and corrosion properties of high-speed laser cladding Fe-based stainless coatings [J]. Journal of Materials Research and Technology, 2024, 29: 3380-92.
55. XU L, YUAN G. The theory and application of nanosecond Laser surface treatment technology: A review [J]. Materials Science and Technology, 2025, 41(14): 989-1021.
56. SAMANTA A, HUANG W, PARVEG A, et al. Enabling Superhydrophobicity-Guided Superwicking in Metal Alloys via a Nanosecond Laser-Based Surface Treatment Method [J]. ACS Appl Mater Interfaces, 2021, 13(34): 41209-19.
57. LI N, LIU W, WANG Y, et al. Laser Additive Manufacturing on Metal Matrix Composites: A Review [J]. Chinese Journal of Mechanical Engineering, 2021, 34(1).
58. XU J, WU Z, NIU J, et al. Effect of Laser Energy Density on the Microstructure and Microhardness of Inconel 718 Alloy Fabricated by Selective Laser Melting [J]. Crystals, 2022, 12(9).

 doi:10.20944/preprints202604.1299.v1

59. CHEN B, ZHONG Y, LI W, et al. Investigation of the Microstructure and Mechanical Performance of GH4099 Alloy Fabricated by Selective Laser Melting [J]. Materials (Basel), 2025, 18(10).
60. DWIVEDI A, KHURANA M K, BALA Y G, et al. Effect of heat treatment on microstructure and mechanical properties for laser powder bed fusion of nickel-based superalloy: A review [J]. Materials Today: Proceedings, 2024, 115: 280-8.
61. LI Y, XU J, LIU B, et al. Adaptation of a heat-treatment condition to a precipitation-hardened nickel-based superalloy produced by laser powder bed fusion [J]. Materials Science and Engineering: A, 2024, 899.
62. WANG R, WANG M, GAO S, et al. Compound purification of nickel base superalloy cutting waste through special cleaning agent attached to ultrasonic stirring [J]. Journal of Cleaner Production, 2022, 378.
63. RAKOCZY Ł, GRUDZIEŃ-RAKOCZY M, HANNING F, et al. Investigation of the γ′ Precipitates Dissolution in a Ni-Based Superalloy During Stress-Free Short-Term Annealing at High Homologous Temperatures [J]. Metallurgical and Materials Transactions A, 2021, 52(11): 4767-84.
64. BASTOLA N, JAHAN M P, RANGASAMY N, et al. A Review of the Residual Stress Generation in Metal Additive Manufacturing: Analysis of Cause, Measurement, Effects, and Prevention [J]. Micromachines (Basel), 2023, 14(7).
65. ZHANG Z, HAN Q, LIU Z, et al. Combined effects of heat treatment and TiB2 content on the high-temperature tensile performance of TiB2-modified Ni-based GH3230 alloy processed by laser powder bed fusion [J]. Materials Science and Engineering: A, 2022, 861.
66. TAN Z H, WANG X G, DU Y L, et al. Temperature dependence on tensile deformation mechanisms in a novel Nickel-based single crystal superalloy [J]. Materials Science and Engineering: A, 2020, 776.
67. XU K, JIANG H, YAN J B, et al. Tensile properties and deformation mechanisms of a solution treated Ni–Fe-based alloy at high temperatures [J]. Materials Science and Engineering: A, 2023, 881.
68. BAI J M, ZHANG H P, LIU J T, et al. Temperature dependence of tensile deformation mechanisms in a powder metallurgy Ni–Co–Cr based superalloy with Ta addition [J]. Materials Science and Engineering: A, 2022, 856.
69. LEI Y, LI X, SUN R, et al. Effect of sintering temperature and heat treatment on microstructure and properties of nickel-based superalloy [J]. Journal of Alloys and Compounds, 2020, 818.
70. LIPPOLD J C, VALIENTE BERMEJO M A, FINK C, et al. Cracking Phenomena in Welding and Additive Manufacturing V [M]. 2026.
71. LI Y M, TAN H B, TAN Z H, et al. Deep insights into damage mechanisms and fatigue life prediction models for a Ni-based single crystal superalloy at different temperatures [J]. Engineering Failure Analysis, 2026, 184.
72. WANG L, SHEN L, YI J, et al. Prediction model of dynamic fracture toughness of nickel-based alloys: combination of data-driven and multi-scale modelling [J]. European Journal of Mechanics—A/Solids, 2026, 116.
73. ZOU T, GUO X, ZHANG Q-Y, et al. Deformation behavior of as-cast Ni-based superalloy under wide temperature range with low strain rates [J]. China Foundry, 2026.
74. ZHOU Q, DING Q, GAO Y, et al. Achieving superplasticity in a hard-to-deform precipitation strengthened Ni-based alloy by suppressing grain boundary brittleness [J]. Acta Materialia, 2026, 304.
75. MA Y, LI Y, OU M, et al. A review on microstructural stability regulation in nickel-based superalloys: synergistic effects of alloying elements and phase stability optimization [J]. Journal of Materials Science, 2025, 60(22): 9024-67.